2014
23rd International Lightning Detection Conference
18 - 19 March • Tucson, Arizona, USA
5th International Lightning Meteorology Conference
20 - 21 March • Tucson, Arizona, USA

Electrification of supercell convection related to polarimetric radar data

Levi D. Boggs
Department of Earth and Atmospheric Science
University of Nebraska - Lincoln
Lincoln, NE

Matthew S. Van Den Broeke
Department of Earth and Atmospheric Science
University of Nebraska - Lincoln
Lincoln, NE

ABSTRACT

Thunderstorm electrification leading to lightning remains relatively poorly-understood. The focus of this study is to compare lightning evolution and electrification for the supercell thunderstorm on 31 May 2013 near El Reno, Oklahoma with the the polarimetric radar variables. Lightning flash rates and flash initiation locations for cloud-to-ground (CG) and intra-cloud (IC) lightning are compared with polarimetric radar data at different stages for the thunderstorm. From the polarimetric radar data, relationships between lightning characteristics and hydrometeor distributions are assessed. An additional emphasis of the study is to examine microphysical changes occurring at the onset of thunderstorm electrification, which may make charge separation more efficient.

I. INTRODUCTION AND BACKGROUND

The most common thunderstorm charging mechanism noted in the literature is the non-inductive charging mechanism, which relies on the riming of graupel from ice crystals in the presence of super-cooled water (Saunders 1993). Many severe storms have very high total flash rates while the CG rate is low, thus having a very high IC:CG ratio. CG flashes in severe storms are often not associated with the regions having the highest reflectivity (> 60 dBZ) as these regions are located where strong vertical development exists (Lang and Rutledge 2002). Weiss et al. (2008) found IC flashes to initiate and propagate within areas of large radar reflectivity values and deepest reflectivity cores. Calhoun et al. (2013) found that flash initiation points cluster in areas near updraft cores, where sedimentation and wind shear produce gradients in charged particles creating electric field magnitudes great enough to initiate lightning. Calhoun et al. (2008) also found the greatest charging rates to be expected in and around updrafts, where mixed-phase regions of supercooled water and riming graupel are present. Palucki et al. (2011) found that in two different thunderstorm cells, the flash-producing cell had critical updraft volumes nearly an order of magnitude larger than a cell without flashes. Carey and Rutledge (2000) found that reflectivity values greater than 30 dBZ must exist at temperatures between 0° and 20°C for a specified time before strong electric fields and lightning can occur. Supercell thunderstorms have lightning holes and rings in regions of wet hail growth, which inhibits rebounding collisions necessary for the non-inductive charging mechanism. Rings of lightning activity are related to Z_{DR} and ρ_{HV} rings thus inferring that lightning rings are associated with charged particles flowing around the mesocyclone (Calhoun et al., 2008). Payne et al. (2010) found that lightning did not follow where the Z_{DR} rings contained values greater than 3 dB, as this part of the ring was likely made of large drops that were not charged. On 31 May 2013 a supercell thunderstorm traversed near the town of El Reno, Oklahoma, producing an EF-5 tornado and total lightning flash rates of around 1300 per minute during the times of 2200 UTC until approximately 0200 UTC on 1 June. This paper will focus on intra-cloud (IC) and cloud-to-ground (CG) flash locations and flash rates related to the polarimetric radar variables. We will analyze microphysical properties of storm cells with large lightning flash rates, adjacent storm cells with low lightning flash rates, and lightning during the onset of thunderstorm electrification. Lightning flash locations compared to differential reflectivity (Z_{DR}) and copolar correlation coefficient (ρ_{HV}) rings will be discussed. Ease of U

II. SYNOPTIC OVERVIEW

On 31 May 2013 a mid to upper level trough was over the central United States, dipping down into the southern Great Plains. High levels of vorticity were advected down into the southern Great Plains from the time period of 1200 UTC 31 May 2013 to 0000 UTC 01 June 2013 with values around 20 x 10^{-5} s^{-1}. A stationary front was located running through northwest Texas and western Oklahoma with a drastic change in wind direction along the front; winds above the front were out of the northeast and winds below the front were from the south to southeast. Convection initiated along a dryline that was located just to the southeast of the stationary front. The dryline was evident from large dewpoint gradients in the area with small dewpoint depressions to the southeast and large dewpoint depressions to the northwest. From a sounding that was launched at 0000 UTC 01 June 2013 from the KOUN station in Norman, Oklahoma(which is approximately 46 miles from El Reno, OK) there was a strong inversion from 850mb to 800mb. The SWEAT index was at 595.5 which indicated a very strong possibility for tornadic activity as any value above 400 indicates tornadoes are possible. The convective available potential energy(CAPE) was 3404 Jkg^{-1} with a lifting condensation level of roughly 1400 meters which is common for tornadic activity. Another good indicator on possible tornadic activity is the Storm Relative Environmental Helicity(SREH), which the sounding mentioned above indicated a value of 418 m^2s^{-2}. High values of SREH indicate that the environment favors thunderstorms capable of strongly rotating updrafts, which are often associated with supercell thunderstorms and tornadoes.

III. METHODS AND DATA

The radar data was collected from the Weather Surveillance Radar 1988-Doppler (WSR-88D) site in Norman, Oklahoma (KTLX), which has polarimetric capabilities. The radar data was obtained from the National Climatic Data Center archive and was displayed using the NCAR-UNIDATA Interactive Data Viewer (IDV) software and Gibson Ridge Analyst 2.0 software. The lightning datasets were obtained from Earth Networks Total Lightning Network (ENTLN) which contained the latitude, longitude, polarity, peak amperage, and time of the lightning strikes for both IC and CG strikes. The lightning sensors from ENTLN use a broad frequency range extending from 1 Hz to 12 MHz that detects both IC and CG lightning. The sensors use GPS technology and algorithms on the entire waveform for every stroke to get an accurate location and classification of IC and CG strikes. The CG strikes were displayed on radar imagery at an elevation angle of 0.9˚ and IC strikes were displayed on radar imagery from either an elevation angle of 2.4˚ or 5.1˚, depending on how far the storm was from the radar during the analysis time. By calculating the time at which the particular elevation angle was being scanned by the radar in each volume scan, the time resolution of the lightning locations could be reduced to smaller intervals to yield more accurate locations. The lightning locations overlaid on radar Plan Position Indicators (PPIs) were from 1 minute intervals for CG strikes and 15 second intervals of IC strikes. The intervals began when the particular elevation angle was being scanned, not at the start of each volume scan. The differing durations was chosen to include enough strike locations for CG lightning and reduce the amount of strike locations for IC to clearly see the radar imagery. The analysis times for this study were divided into 3 different intervals consisting of four volume scans each which is shown in Table 1: two intervals when both the CG and IC flash rates were increasing, and a time where both flash rates were nearly constant. To determine the environmental freezing level, the sounding on 0000 UTC 01 on June 2013 from the weather station KOUN in Norman, Oklahoma was used.

IV. RESULTS AND DISCUSSION

A. Cloud-to-Ground vs. Intra-Cloud

a) Time 1(initial flash rate increase)

From Fig. 2, the majority of CG strikes took place in regions A and C throughout this analysis time. The flash rate increased dramatically during this time period, from around 30 strikes min^{-1} at the start of time 1, to around 95 strikes min^{-1} at the end of time 1 (Fig. 1). A majority of CG strikes took place outside the areas of highest reflectivity, often occurring in regions of 45 to 55 dBZ. Very few strikes were located inside regions greater than 60 dBZ. The CG strikes seemed to occur in the highest gradients of reflectivity.

The IC strikes during this time had the highest strike densities regions A and C from Fig. 2, similar to the CG strike information. At the start of time 1, the IC flash rate was around 300 flashes min^{-1} and at the end of time 1 the flash rate was around 850 flashes min^{-1} (Fig. 1). The IC strikes were found adjacent to areas of highest reflectivity, in areas greater than 60 dBZ. In region A, the amount of IC flashes decreased throughout time 1. The areas of highest reflectivity in this region also decreased, with the fourth volume scan during time 1 (2237 UTC) showing a significant reduction in areas with high reflectivity, being dominated by values around 45 dBZ. In region C, the areas of highest reflectivity and flash rate increased throughout time 1. Many of the strikes were located on the edges of highest reflectivity values, on the border of roughly 60 to 65 dBZ values. Many strikes were in regions with the highest reflectivity values.

TABLE 1.

Analysis time	**Actual time and date**	**Description**
Time 1	2219 : 2237 UTC 31 May 2013	Initial electrification and storm development, IC and CG flash rates show steep increases.
Time 2	0005 : 0023 UTC 01 June 2013	IC and CG flash rates show a steep increases. The storm is in a mature phase.
Time 3	0055 : 0114 UTC 01 June 2013	High IC flash rate, low CG flash rate, both rates nearly constant. Storm is in a mature phase

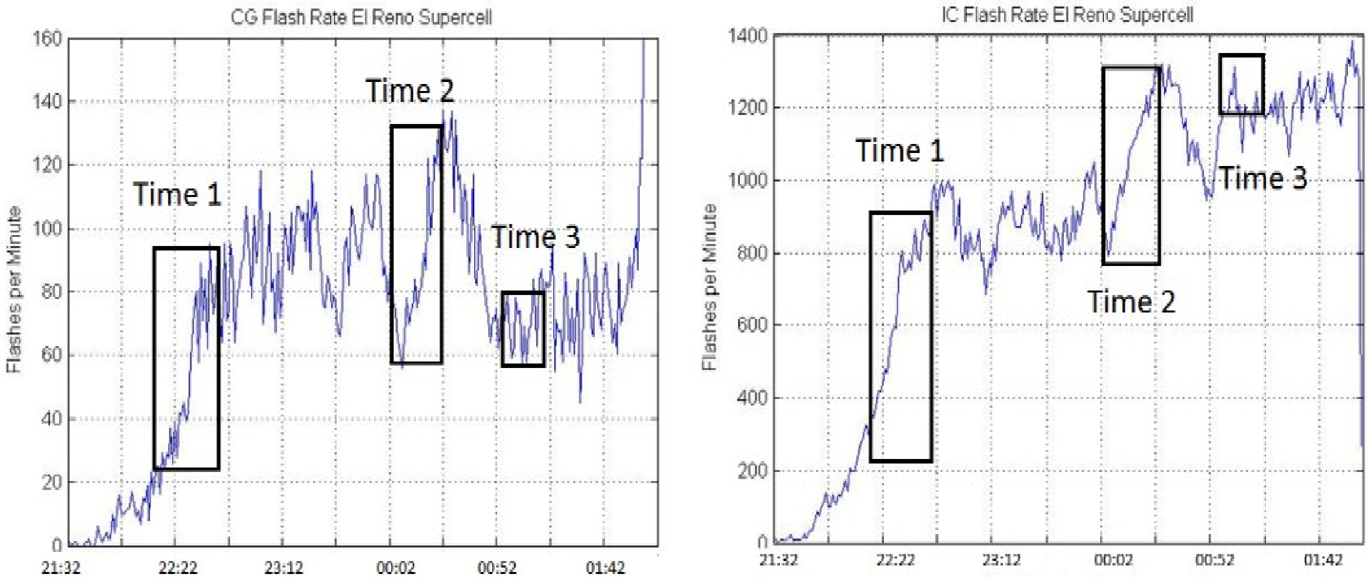

Fig. 1. CG and IC flash rates throughout the storm. Times 1,2, and 3 are marked in the square boxes.

b) Time 2(supercell mature)

From Fig. 1, this analysis time had the CG flash rate starting with 65 flashes min^{-1} and ended with 125 flashes min^{-1}. This time contained the overall maximum in the CG flash rate for the entire storm life cycle, with a flash rate of 125 flashes min^{-1} near the end of time 2. According to Fig. 3, the CG strikes occurred in areas of moderate reflectivity, around 50 dBZ. There were very few strikes in areas with reflectivity less than 50 dBZ or greater than 60 dBZ. Region A had a minor increase in the number of strikes per volume scan, with areas of moderate and high reflectivity remaining fairly constant. Region C started off with very few strikes in the first volume scan while the amount of strikes dramatically increased until the end of time 2. The areas of reflectivity greater than 60 dBZ also increased during this time, which can be linked to more updrafts being found in this area as time increases. Strikes took place in regions with reflectivity 50-59 dBZ in gradients of reflectivity.

The IC flash rate started around 800 flashes min^{-1} and ended around 1200 flashes min^{-1} during time 2. The ending flash rate of around 1200 flashes min^{-1} was near the overall maximum flash rate of the entire storm study period. In region A, the flashes took place mainly around the areas of highest reflectivity, however there were a few strikes in regions of low reflectivity, around 20 dBZ. The amount of strikes in this region increased rapidly throughout time 2, different from the CG strike information. Region C showed IC strikes taking place in areas of highest reflectivity. The amount of strikes throughout time 2 in this region remained nearly constant. The areas of high reflectivity increased throughout time 4, however the IC flashes did not increase as the CG flashes did in this region.

c) Time 3(supercell mature)

From Fig. 4, this analysis time only contained region A, as regions B and C had moved to the north east out of the study range. The CG flash rate started out around 75 flashes min^{-1}, and decreased to around 65 flashes min^{-1} during this time period. The CG flashes were restricted to the areas of moderate reflectivity (40 to 45 dBZ) and on edges of the highest reflectivity (60 dBZ).

The IC flash rate remained around 1200 flashes min^{-1} for this time period. The majority of flashes occurred on the eastern side of the storm, where high reflectivity values covered the largest area. During this time period, the IC flash rate was still around its overall maximum, while the CG flash rate decreased significantly.

B. Lightning flash rate related to the polarimetric variables

a) Time 1(initical flash rate increae)

Z_{DR}

From Fig. 5, the CG flashes occurred on the edges of high Z_{DR} (around 4-5 dB). There were very few strikes in region B of the storm, with lower Z_{DR} values there. The highest number of strikes occurred in areas surrounding the highest values of Z_{DR}, which occurred in regions A and C. Throughout time 1, the region A showed strikes occurring on edges of the largest Z_{DR} gradients. The large gradients of Z_{DR} around high values of Z_{DR} are indicative of liquid updraft cores surrounded by mixed phase particles, which include frozen hydrometeors. Strikes were generally not located inside the regions of highest Z_{DR}, as these areas were located inside updrafts with high vertical velocities discouraging charge separation by sedimentation. The area of highest Z_{DR} values seemed much larger in the last volume scan with the high flash rate when compared with the first volume scan and low flash rate. This can be related to larger vertical velocities in these updrafts which have created more oblate liquid hydrometeors. Region C also had strikes on the highest Z_{DR}

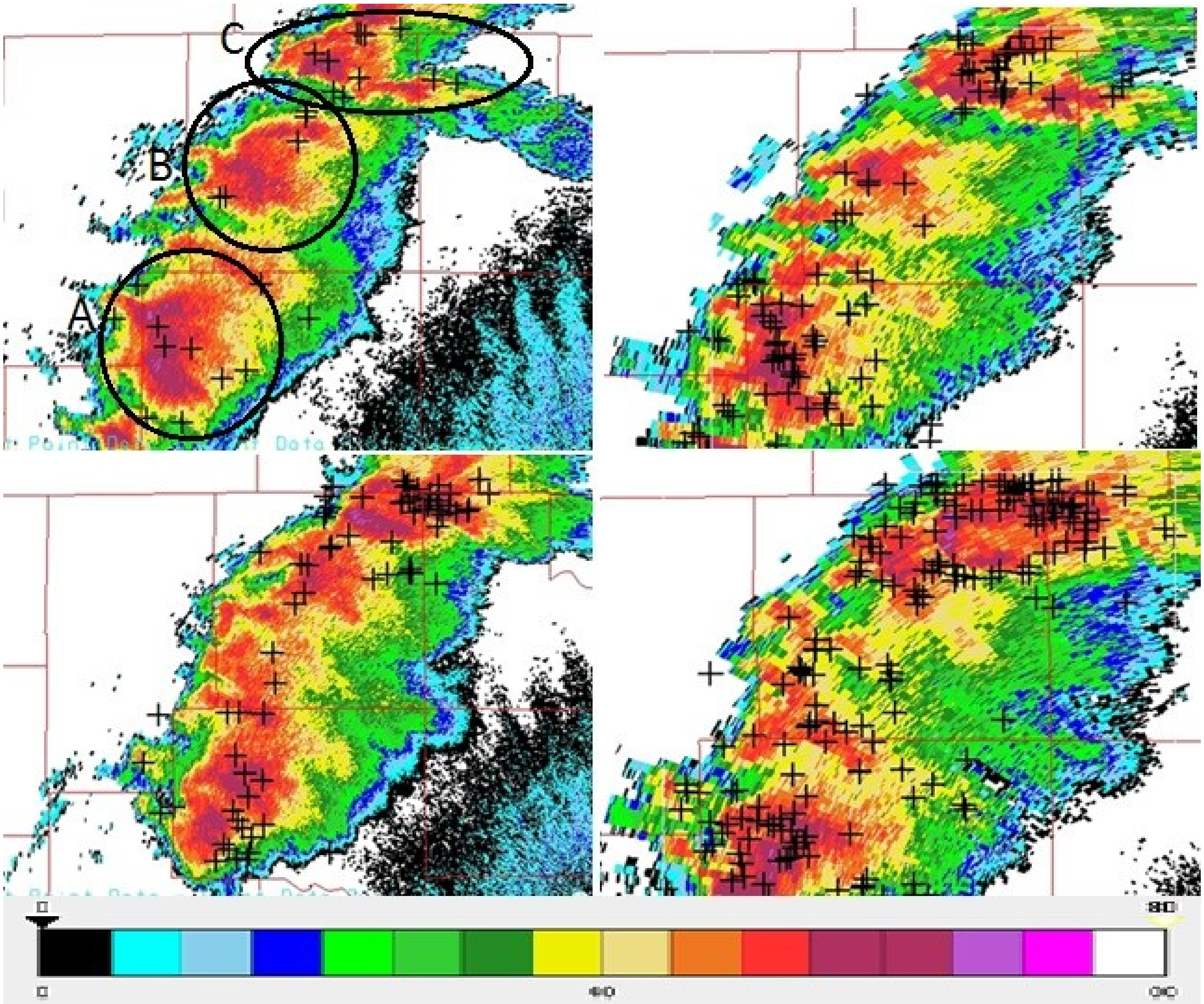

Fig. 2. The left side shows CG strikes during time 1 and the right side shows IC strikes during time 1. The top images are from the first volume scan and the bottom images are from the last volume scan. Regions A, B, and C apply to all images in Fig. 2. The reflectivity is displayed in dBZ.

gradients, with few strikes inside the contours of highest Z_{DR}. The first volume scan showed strikes spread out around areas of high Z_{DR}, while the last volume scan showed strikes clustered together closely north west of a cyclonically curved feature with high Z_{DR}. The high strike density there could have been from charged particles being advected around the mesocyclone there, falling out to the north west creating large charge separation and initiating CG strikes.

According to Fig. 5, IC lightning occurred in regions of low Z_{DR}, around -1 to 0 dB at an elevation angle of 2.4˚. However, the strikes were near areas of enhanced Z_{DR} with values around 4 to 5 dB which implied Z_{DR} columns extending above the freezing level, considering the local Z_{DR} maximums were located in low to negative Z_{DR} values. The areas of highest flash densities occurred around these Z_{DR} maxima. Region A showed two local maxima in Z_{DR}, with strikes taking place on the edges of these maxima alongside the low Z_{DR} during volume scans 2 and 3. Volume scan 4 (Fig. 5) showed a ring-like feature of enhanced Z_{DR} that will be discussed in another section for the southern region. Region A showed two areas of locally higher Z_{DR} values. IC flashes started out located between these two Z_{DR} maxima. Volume scans 3 and 4 for this region showed the strikes connecting the two maxima in Z_{DR}, with flashes initiations beginning on edges of high Z_{DR} and following Z_{DR} pixels around -1 dB between the two maximums. The number of strikes increased as the distance between the two Z_{DR} maxima increased, with the distance between the two Z_{DR} maxima increasing with each successive volume scan.

ρ_{HV}

CG flashes occurred on ρ_{HV} gradients. The strikes were mainly located within ρ_{HV} around 0.95, however a few took place in ρ_{HV} as low as 0.7. For region A (Fig. 6), the first volume scan with the low flash rate had a large area of low ρ_{HV} surrounded by high ρ_{HV}, while the last volume scan with the high flash rate showed a smaller area of low ρ_{HV} but a

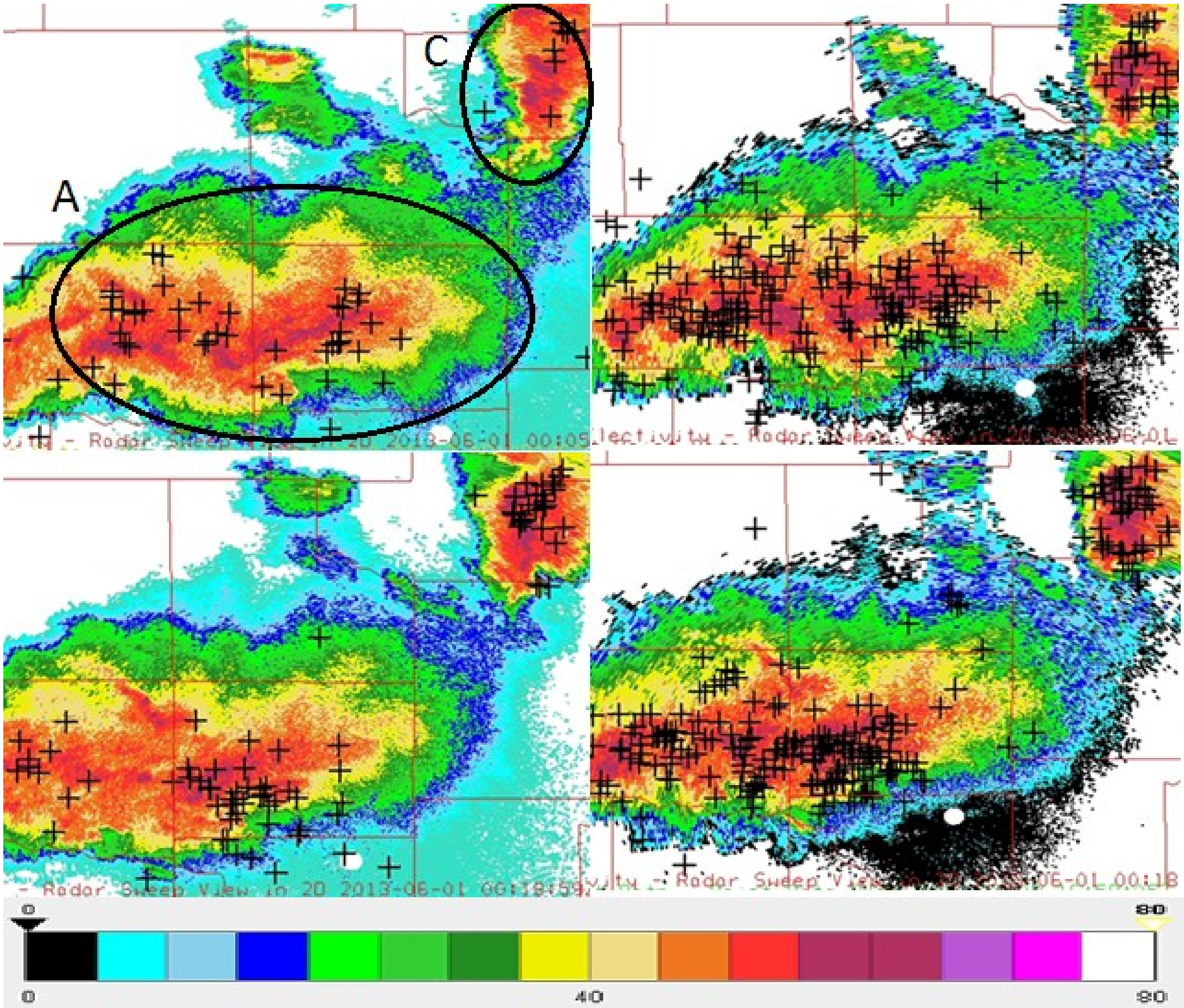

Fig. 3. The left side shows CG strikes during time 2 and the right side shows IC strikes during time 2. The top images are from the first volume scan and the bottom images are from the last volume scan. Regions A and C apply to all images in Fig. 3. The reflectivity is displayed in dBZ.

larger area with variable ρ_{HV} values. Region C also showed strikes on the borders of high and medium ρ_{HV}. The largest number of strikes occurred in the last volume scan of this time period and were located in a region characterized by a large spread of ρ_{HV} values. Throughout this time period the area of highly variable ρ_{HV} values increased with each volume scan, as did the flash rate. This inferred that the regions of mixed phase particles was increasing during this time period.

The IC flashes occurred mainly in areas of high ρ_{HV}, although the data at this elevation angle of 2.4˚ was noisy for ρ_{HV}. High Z_{DR} in region A from Fig. 5 at this time corresponded to values of low ρ_{HV} in Fig. 6, with the low ρ_{HV} being on the edges of high Z_{DR}. The low ρ_{HV} on the periphery of high Z_{DR} values implied that mixed phase particles were on the edges of updraft regions. The mixed phase particles are key for the non-inductive charging mechanism as the interactions of frozen hydrometeors and supercooled water are required to create charge under this mechanism. The mixed phase particles would have been in regions with large vertical velocity gradients as they were on the edge of updrafts, which would encourage sedimentation of hydrometeors carrying charge, encouraging flashes. There was a larger spread of ρ_{HV} values with the last volume scan when compared with the first volume scan. Region C also showed strikes around large ρ_{HV} gradients. The strikes cluster on edges of low ρ_{HV}, but took place in areas of high to moderate ρ_{HV} with values around 0.90 to 0.95. The last two volume scans showed the strikes following ρ_{HV} values slightly depressed from the environment, with values around 0.90 to 0.92. These paths corresponded to the depressed Z_{DR} values discussed previously.

K_{DP}

The CG flash locations took place near areas of moderate (2 deg km^{-1}) and high (6 deg km^{-1}) K_{DP} from Fig. 7. Regions A and C showed larger areas of high K_{DP} which correlated with larger numbers of strikes in those regions. Region A had strikes clustered near values of 2 to 3 deg km^{-1}. Region C had strike locations surrounding areas of high K_{DP}, with the locations found on the borders of high and low K_{DP}. The area of highest K_{DP} increased with each successive volume scan as did the number of CG strikes in this region.

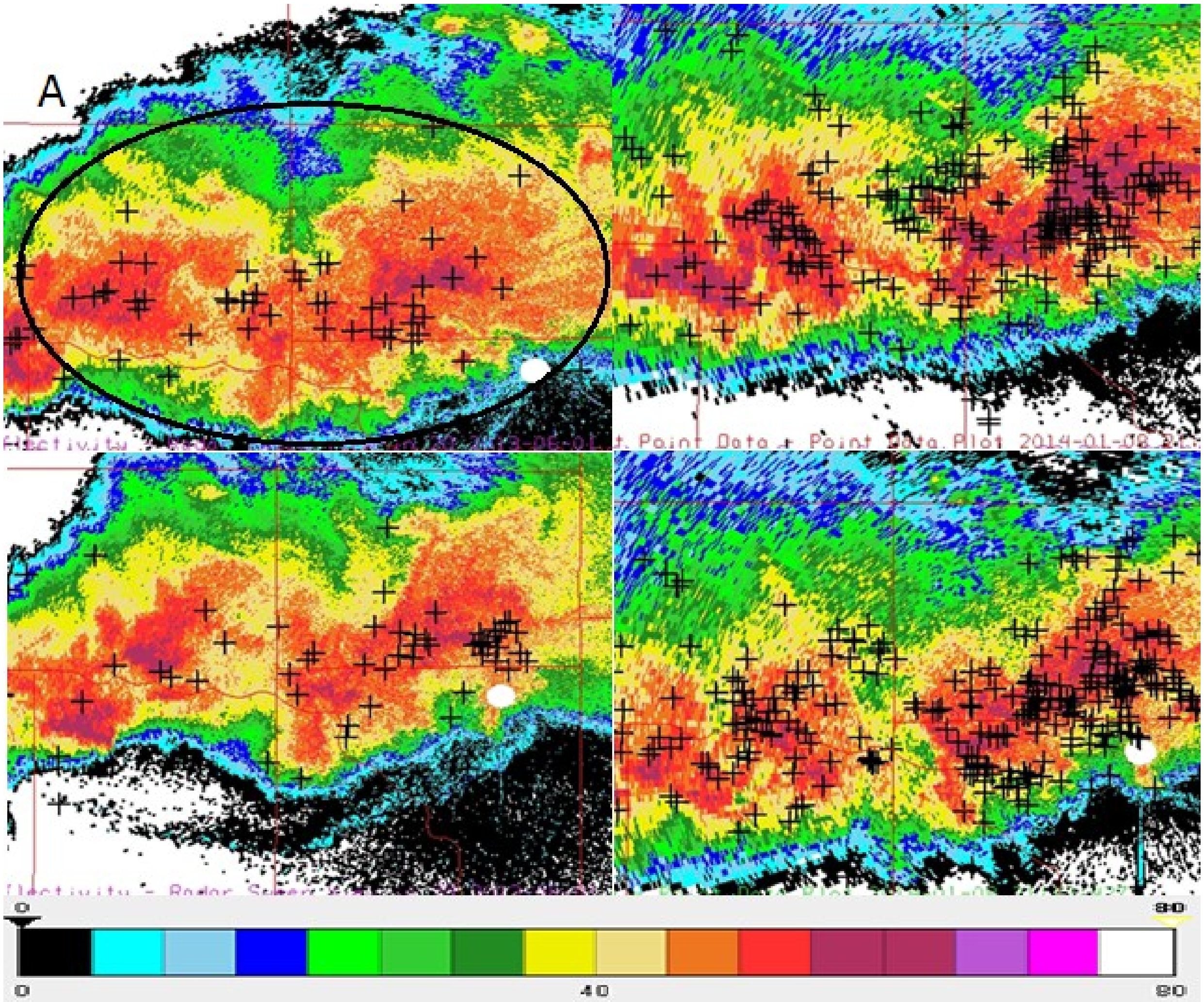

Fig. 4. The left side shows CG strikes during time 3 and the right side shows IC strikes during time 3. The top images are from the first volume scan and the bottom images are from the last volume scan. Region A applies to all images in Fig. 4. The reflectivity is displayed in dBZ.

This can be related to larger areas of intense updrafts as the storm developed. Flashes were not located in regions of the highest K_{DP}, as strong updrafts indicated by the high K_{DP} contained large vertical velocities discouraging charge separation.

IC flashes were located near regions of high K_{DP}, but within low values of K_{DP}. The flash locations were well-correlated with strong K_{DP} gradients. For region A from Fig. 7 for IC strikes, the area of highest K_{DP} values and number of IC flashes increased with time. The last volume scan had a circular area of high K_{DP} with values around 6 degrees km^{-1}, and the highest density of flashes took place around this local maximum in K_{DP}. The high K_{DP} at this elevation angle (2.4˚) implied liquid water above the freezing level, which larger amounts of this on edges of intense updrafts should lead to greater charge generation and separation. The first volume scan did not have this feature of enhanced K_{DP} and the high flash density was also absent from the first volume scan. Region C had small areas of moderate to high K_{DP} in the first volume scan, while these areas increased with time. The flash amount also increased with time in this region and the strike locations took place around areas of high K_{DP}.

b) Time 2(supercell mature)

Z_{DR}

During this time period, CG strikes occurred on large Z_{DR} gradients (around 1 to 4 dB). From Fig. 8, for region A, the majority of the CG strikes occurred on the eastern side which was characterized by the largest area of high Z_{DR} values. Similar to time 1, very few strikes were located inside the regions of highest Z_{DR}, however, the borders of high Z_{DR} were positively correlated with strike locations. This region had a number of strikes nearly constant with each volume scan, though flash rate increased in the northern region. Region C had CG strikes on the periphery of the area with the largest Z_{DR} values, which was around 5 dB. Through time, this region of highest Z_{DR} increased substantially, as well as the amount of strikes in this region. The last volume scan showed a dense cluster of strikes initiating to the northwest of this region of high Z_{DR}. Ice particles indicated from the low Z_{DR} values were located around high Z_{DR} values and were likely charged and advected to the north west, underwent

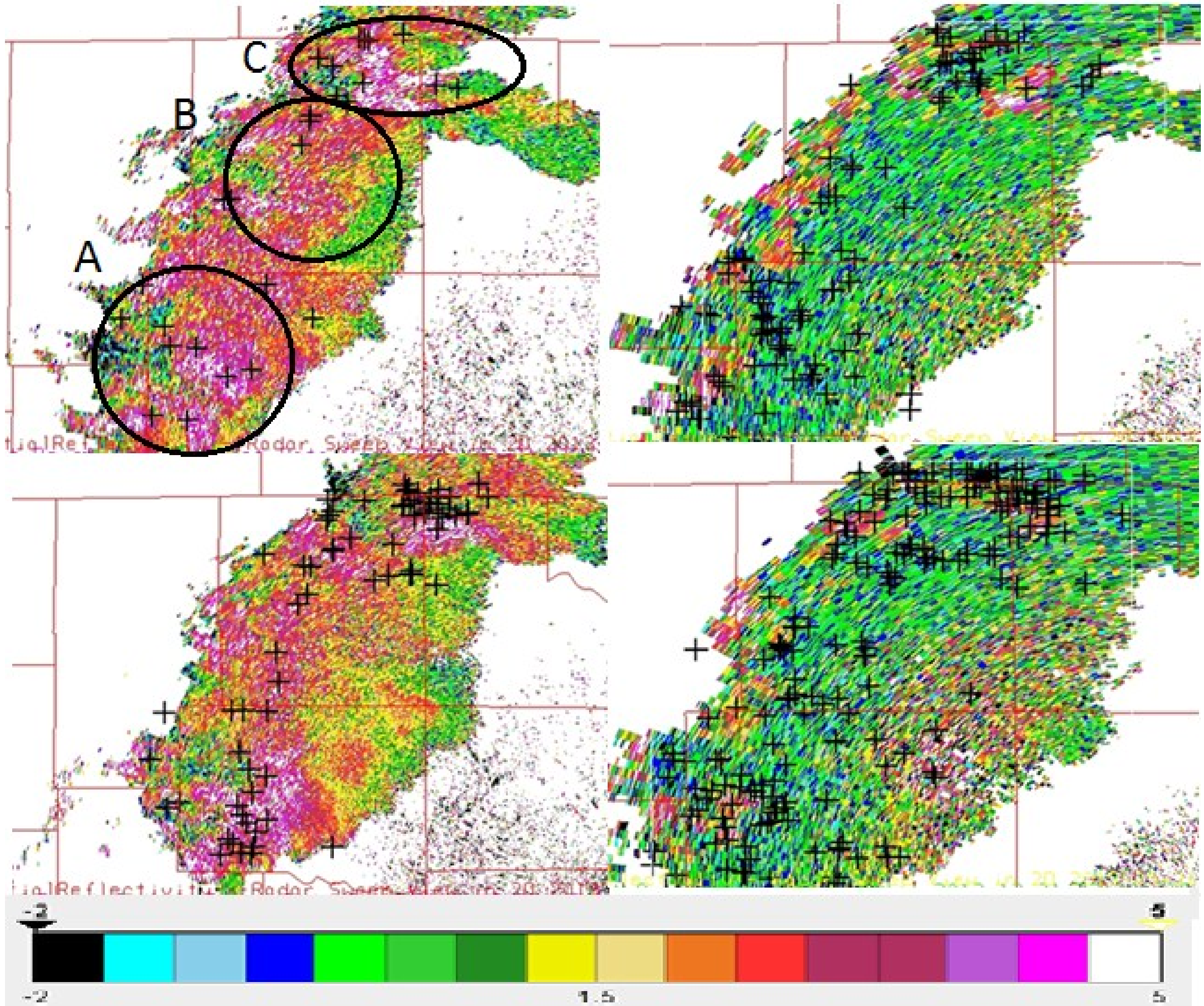

Fig. 5. The left side shows CG strikes during time 1 and the right side shows IC strikes during time 1. The top images are from the first volume scan and the bottom images are from the last volume scan. Regions A, B, and C apply to all images in Fig. 5. The units are in dB.

sedimentation as they were on the edge of the updraft and initiated CG strikes.

Region A for IC flashes had locations of strikes at variable Z_{DR} values at an elevation angle 2.4˚ (Fig. 8). This was partially due to the storm being very close to the radar. The highest flash densities occurred in areas of highest Z_{DR}; many were located in areas with Z_{DR} of 4 to 5 dB. The number of strikes in the eastern part of the storm increased with each successive volume scan and it appeared the mesocyclone in this region was becoming more defined as high Z_{DR} structures were cyclonically curved. Region C had an enhanced area of Z_{DR}, with strikes located to the northwest of this area. The strikes grouped in areas of negative Z_{DR} (-1 dB). The number of strikes in the northern region through each successive volume scan for this analysis time was nearly constant.

ρ_{HV}

The CG flash locations occurred in ρ_{HV}, around 0.95 (Fig. 9). Region A had strike locations on strong ρ_{HV} gradients. Region B during this time period had very noisy data, with large areas of mixed values. The degradation of ρ_{HV} during this time made this variable less reliable. The strikes were located in ρ_{HV} around 0.95, on edges of ρ_{HV} around 0.90.

The IC flashes took place in regions of ρ_{HV} around 0.95, particularly avoiding areas of lower ρ_{HV}. Region A for the IC flashes had the last volume scan with a lower spread in values across this area when compared with previous volume scans. Majority of the strikes took place in higher ρ_{HV} values to the eastern part of the storm. For region C, the strikes took place in higher ρ_{HV}, however strikes were not purely in areas of high ρ_{HV} but rather located in regions with large ρ_{HV} gradients (on the periphery of low ρ_{HV} pixels).

K_{DP}

Most CG strikes took place near areas of enhanced K_{DP}. Region A from Fig. 10 showed the largest density of

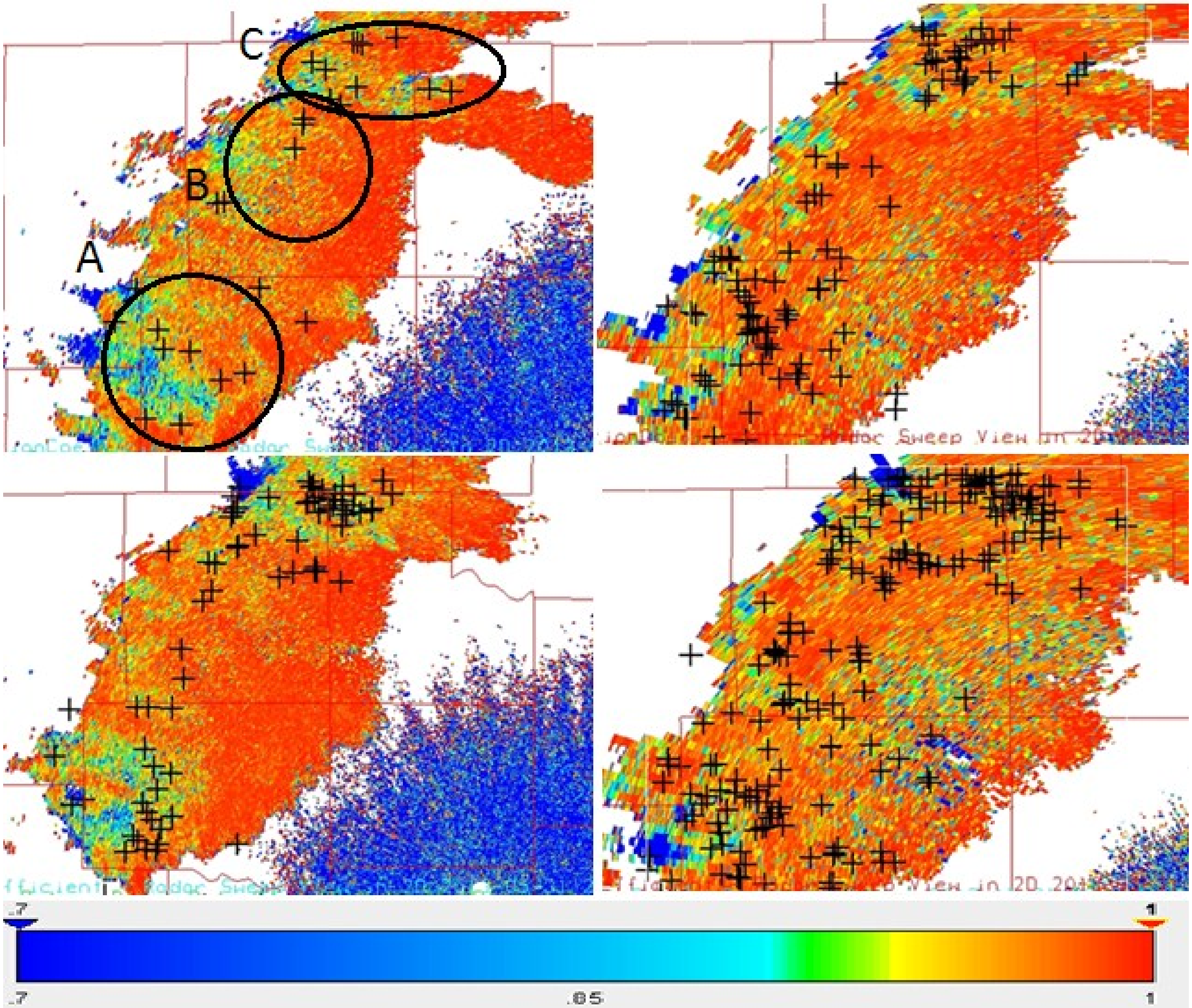

Fig. 6. The left side shows CG strikes during time 1 and the right side shows IC strikes during time 1. The top images are from the first volume scan and the bottom images are from the last volume scan. Regions A, B, and C apply to all images in Fig. 6

strikes clustering to the eastern part of the storm through time. The eastern region of the storm also showed an increased area of high K_{DP} values as time progressed, which is related to the strengthening up the updraft in this region. The western side of the storm had a large number of strikes in the first volume scan which corresponded to a large area of high K_{DP} values and this area of high K_{DP} values decreased with each successive volume scan. The overall number of strikes was nearly constant in region A of the storm during this time period; however, the western side of region A experienced fewer strikes with time while the eastern side of the southern region experienced larger numbers of strikes with time. This was probably because the western side of region A experienced a weaker updrafts while the eastern side of region A showed updrafts strengthening. Region C showed the number of strikes increasing with time with the area of K_{DP} values around 6 deg km^{-1}. The strikes took place not in the areas of highest K_{DP}, but on the periphery of highest K_{DP} values.

The IC flash locations covered a large spread of K_{DP} values, as the majority of flashes took place on the eastern side of the storm (Fig. 10). The number of strikes and K_{DP} values increased with time in regions A and C, which can be related to updrafts strengthening in these regions. The highest strike densities were on the eastern edge of the storm throughout all volume scans and the eastern side of the storm showed the highest areas of K_{DP} for all volume scans.

c) time 3(supercell mature)

Z_{DR}

The CG strikes took place almost exclusively on borders of high Z_{DR}, however the area of high Z_{DR} in region A (Fig. 11) was much less when compared with earlier times 1 and 2. Many of the flash locations were grouped near the areas with the highest Z_{DR}, however no strikes were physically located in the regions of high Z_{DR} but rather on the boundaries

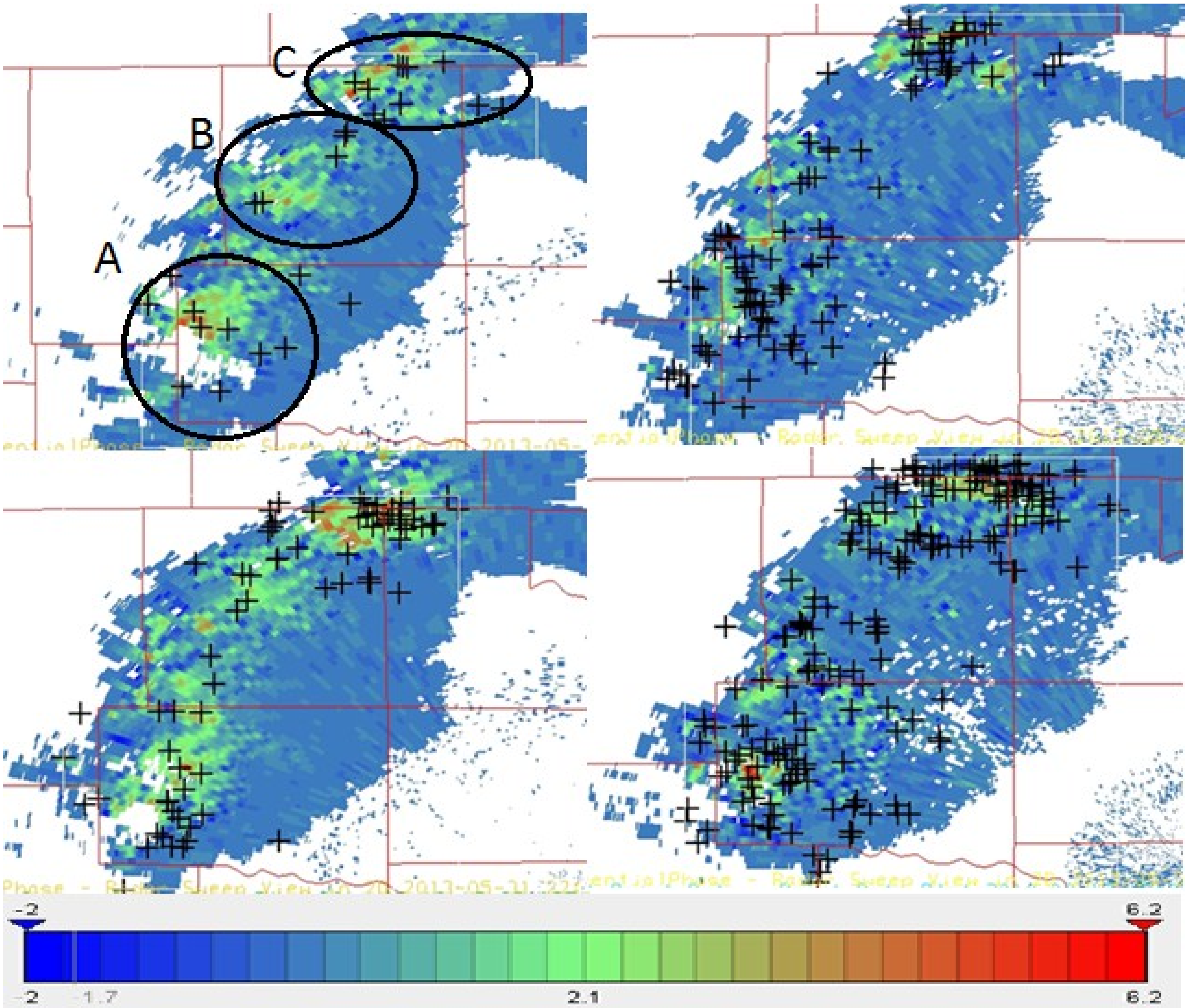

Fig. 7. The left side shows CG strikes during time 2 and the right side shows IC strikes during time 1. The top images are from the first volume scan and the bottom images are from the last volume scan. Regions A, B, and C apply to all images in Fig. 7. The units are deg km^{-1}.

of high and low Z_{DR}, which seem more pronounced during this time. The last volume scan showed a large amount of strikes to the eastern part of the storm and this region was characterized by the largest areas of high Z_{DR}.

From Fig. 11, the IC flash locations were nearly all on the eastern region of the storm during this time. This region had large areas of high Z_{DR} when compared with the western edge of the storm, however this is largely contributed to the altitude of the beam on the western side of the storm as the radar was located to the east of the storm. There was evidence of a well-defined Z_{DR} ring with interesting flash locations near it that will be discussed later. The last volume scan contained a larger area of high Z_{DR} values when compared with the first volume scan, although the flash rate was nearly constant throughout this analysis time. The larger areas of high Z_{DR} were probably attributable to the storm moving closer to the radar with time while the beam passed through more regions at lower elevations, meaning more liquid water returning power to the radar which means higher Z_{DR} estimates.

ρ_{HV}

Fig. 12 showed CG flashes in areas of high ρ_{HV} with values around 0.95. Strikes were however grouped near boundaries of high and moderate ρ_{HV}. Very little strikes occurred in homogeneous areas of high ρ_{HV}; the gradients of ρ_{HV} were prime locations for flash locations. There was little change in the distribution of ρ_{HV} with each successive volume scan for this time.

The locations of IC flashes occurred in moderate values of ρ_{HV} at this elevation while flashes avoided particularly low values of ρ_{HV} (around 0.7). Evidence of a ρ_{HV} ring appeared here and will be discussed later. Flashes tended to be located near the lower ρ_{HV} values, but on the periphery of the areas of low ρ_{HV} and located in the moderate to high values of ρ_{HV}. The distribution and spread ρ_{HV} through each volume scan during this time was nearly constant.

K_{DP}

The amount of CG strikes for this time period was nearly

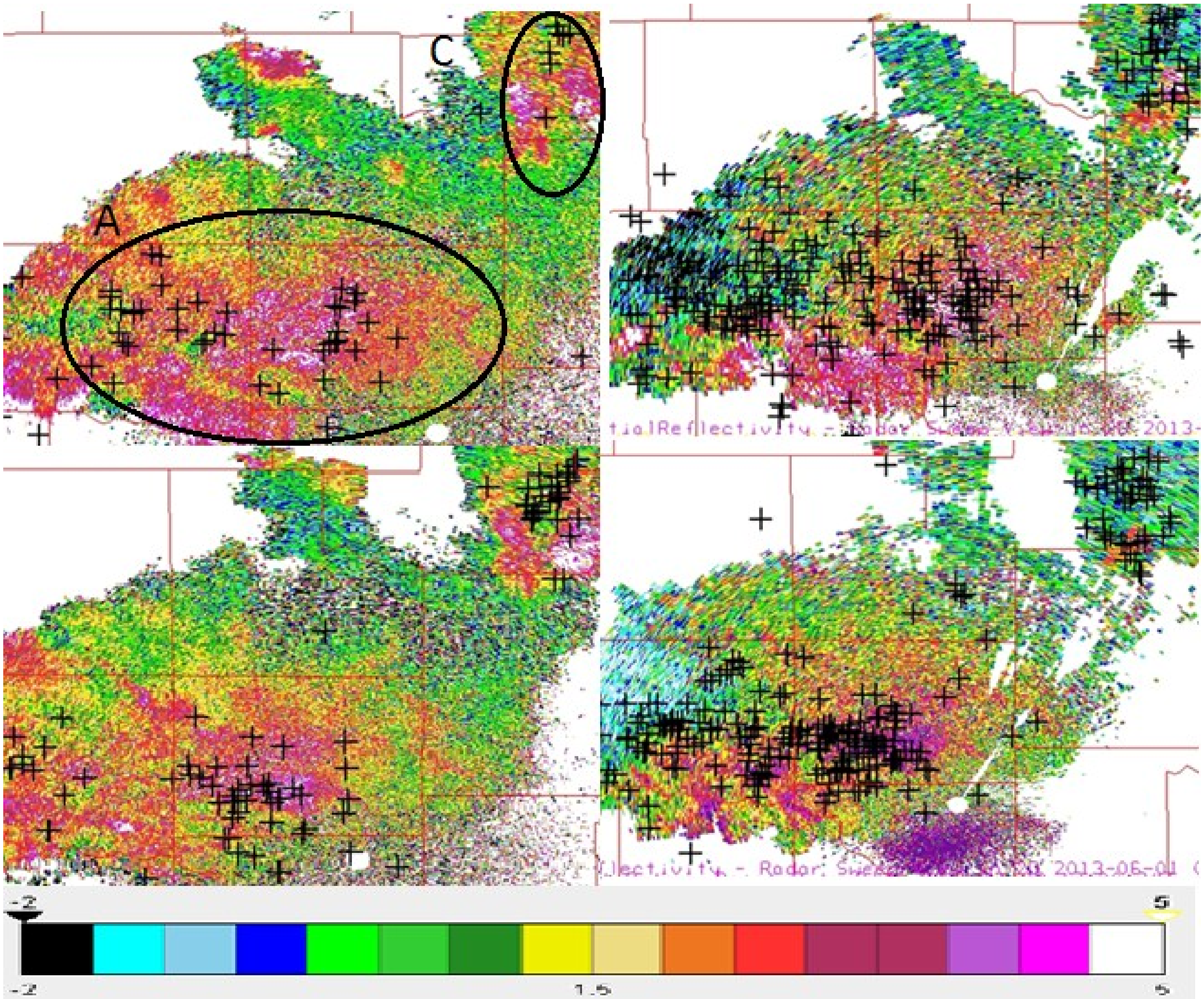

Fig. 8. The left side shows CG strikes during time 2 and the right side shows IC strikes during time 2. The top images are from the first volume scan and the bottom images are from the last volume scan. Regions A and C apply to all images in Fig. 8. The units are dB.

constant and the distribution of K_{DP} was nearly constant as well for this time period (Fig. 13). There was two areas with high K_{DP} values; one on the western edge of the storm and one on the eastern edge. The strikes grouped around high areas of K_{DP}, however the western edge of the storm with high K_{DP} values had little strikes around it towards the end of this analysis time.

The IC flashes had the largest density around the local maximum in K_{DP} which was located to the eastern edge of the storm. This area of high K_{DP} was very large compared to previous analysis times, and the majority of strikes were located around this K_{DP} maximum while little strikes took place inside the maximum. The analysis time contained the highest IC flash rate of the entire study time and this could possibly be linked with this enlarged area of high K_{DP}.

C. Varying lightning activity in adjacent storm cells during the onset of electrification

For this analysis, time 1 was chosen as a time when the storm showed adjacent, separated cells with high reflectivity maxima containing high and low lightning activity. Both the CG and IC flashes showed this pattern of cells with large numbers of lightning strikes next to cells with few lightning strikes. As time progressed, the number of flashes in the adjacent cells increased, even though both cells had quite different lightning activity. The cells analyzed were regions A and B from Fig. 2, as region A showed substantial lightning activity and region B showed very little lightning activity during this analysis time.

From previous studies, the amount of liquid water above the environmental freezing level is thought to be necessary for the non-inductive charging mechanism as this mechanism relies on interactions between supercooled water and ice particles to generate charge (Saunders 1993). For water to be supercooled, it must be below 0°C, which means that liquid water signatures above the environmental freezing level provide a good estimation for the amount of supercooled water in a particular region. Cross sections of Z_{DR} and K_{DP} were analyzed to infer the amount of liquid water above the freezing level. The melting level was found to be at roughly

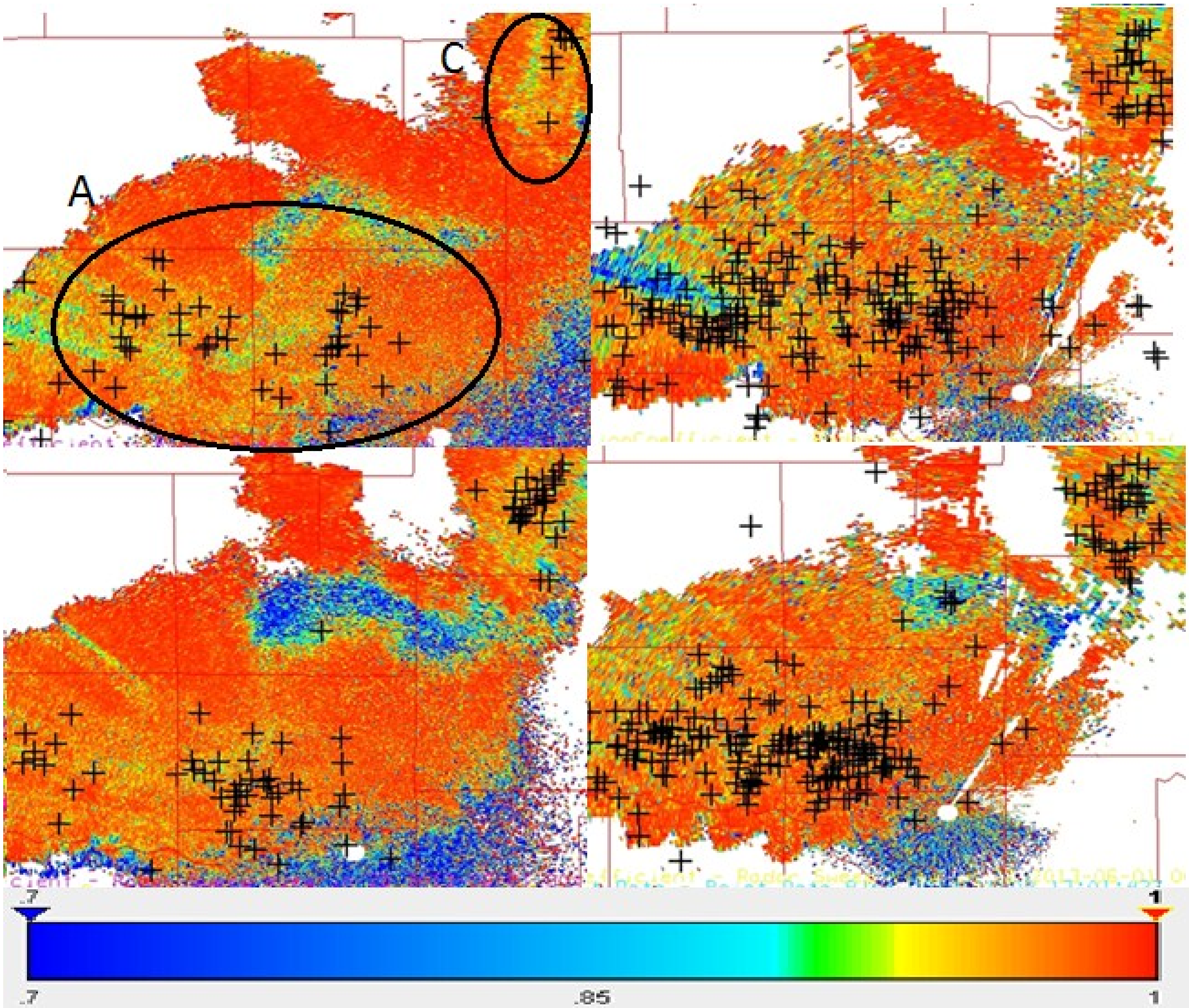

Fig. 9. The left side shows CG strikes during time 2 and the right side shows IC strikes during time 2. The top images are from the first volume scan and the bottom images are from the last volume scan. Regions A and C apply to all images in Fig. 9.

15,270 ft (4.6 km) from the KOUN 0000 UTC 01 June 2013 sounding.

Z_{DR}

The first volume scan showed region A (Fig. 14) have moderate Z_{DR} of 2 to 3 dB to heights of about 18,000 ft and Z_{DR} values around 5 dB to heights of 10,000 to 11,000 ft. Z_{DR} values around 0 to -1 dB were immediately above these areas of enhanced Z_{DR}, which implied frozen hydrometeors. The low Z_{DR} values were located at the top of updraft regions, where small ice nuclei from above can come into contact with the supercooled water from below, creating ice particles in this region. The number of flashes in this region during this volume scan was low compared to the overall flash rate of the entire study time, though this region contained many more flashes than the middle region at this time. This was likely due to a smaller amount of liquid water above the freezing level. The vertical Z_{DR} profile during the last volume scan (Fig. 15) for this analysis time shows Z_{DR} values of 5 dB extending to 20,000 ft. Moderate values of Z_{DR} extend to around 25,000 ft, while low Z_{DR} values were on the periphery of these moderate values of Z_{DR}. The number of strikes in this region during this volume scan was high when compared to the overall flash rate of the entire study time and much higher than the number of flashes in the middle region. The large amount of liquid water above the freezing level resulted in more riming of ice particles located above and on the outside of updrafts, resulting in more charge being generated.

Region B showed moderate values of Z_{DR} (2 to 3 dB) to heights of 25,000 ft, however values of 4 to 5 dB were contained below 8,000 ft during the first volume scan (Fig. 14). Values of -1 dB were above the regions of high Z_{DR}. This region had a low flash rate when compared to other regions during this time and the flash rate of the entire study time. The low amount of liquid water above the freezing level would have inhibited the riming of ice particles with supercooled water, reducing the charge created by the non-inductive charge mechanism. A cross-section at the last volume scan from Fig. 15 rarely showed high Z_{DR} values;

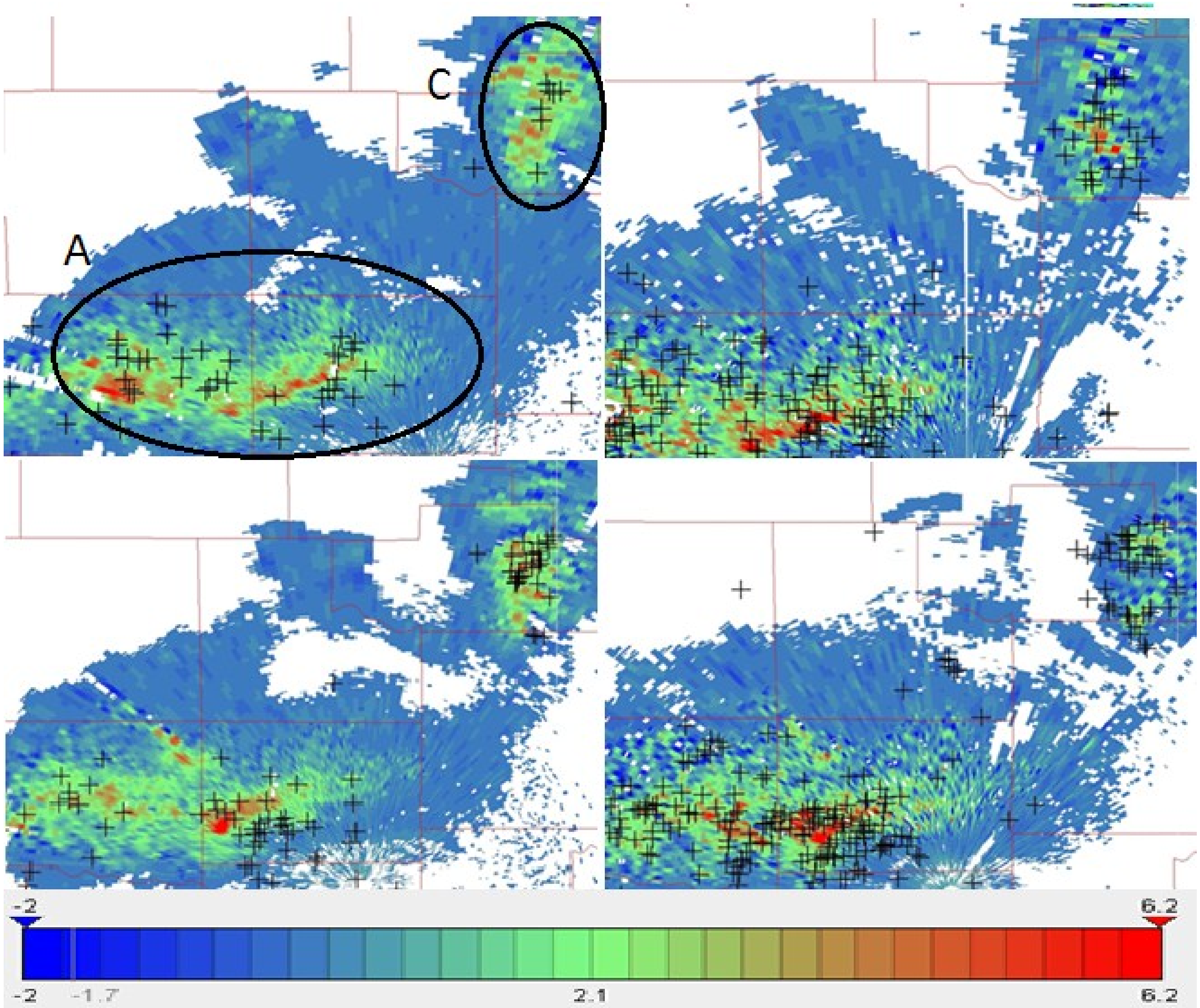

Fig. 10. The left side shows CG strikes during time 2 and the right side shows IC strikes during time 2. The top images are from the first volume scan and the bottom images are from the last volume scan. Regions A and C apply to all images in Fig. 10. The units are deg km^{-1}.

values of 4 to 5 dB extended to roughly 8,000 ft. Moderate values of Z_{DR} extended to roughly 10,000 ft. Low Z_{DR} values were located above the moderate values as before. The flash rate during this volume scan was also very low, however it was higher than the first volume scan for this region.

K_{DP}

Region A from Fig. 14 showed values of K_{DP} around 5 deg km^{-1} extending to heights of 19,000 ft during the first volume scan. This area of high K_{DP} matched well with the area of enhanced Z_{DR}. The last volume scan from Fig. 15 for this region showed K_{DP} values around 5 deg km^{-1} to heights of 25,000 ft. This area of high K_{DP} was also nearly collocated with the area of enhanced Z_{DR} during this time, enforcing that large amounts of liquid water existed above the freezing level.

Region B during the first volume scan (Fig. 14) showed high K_{DP} values extending to roughly 15,000 ft in height. The horizontal extent of these high K_{DP} values was very large, and most of the high values of K_{DP} were contained below 8,000 ft. The last volume scan (Fig. 15) showed high values of K_{DP} up to heights of 10,000 ft but overall the area of high K_{DP} values was relatively small. High K_{DP} values were located well below the freezing level, and the overall area of high K_{DP} values on the cross section was small. This means low values of supercooled water available for the non-inductive charging mechanism.

D. Lightning rings related to the polarimetric variables

Z_{DR}

During time 1, a circular ring of lightning strikes was well-correlated to high Z_{DR} values, around 4 to 5 dB (Fig. 16). The strikes were primarily on the outside of this ring-like feature. No lightning points were located in any high Z_{DR} pixels but rather in the Z_{DR} values of 0 to -1 dB on the periphery of the ring, which is consistent with the results of Payne et al. (2010). This ring-like feature was only present during the last volume scan of time 1. The ring of enhanced Z_{DR} and lightning flashes persisted throughout each volume

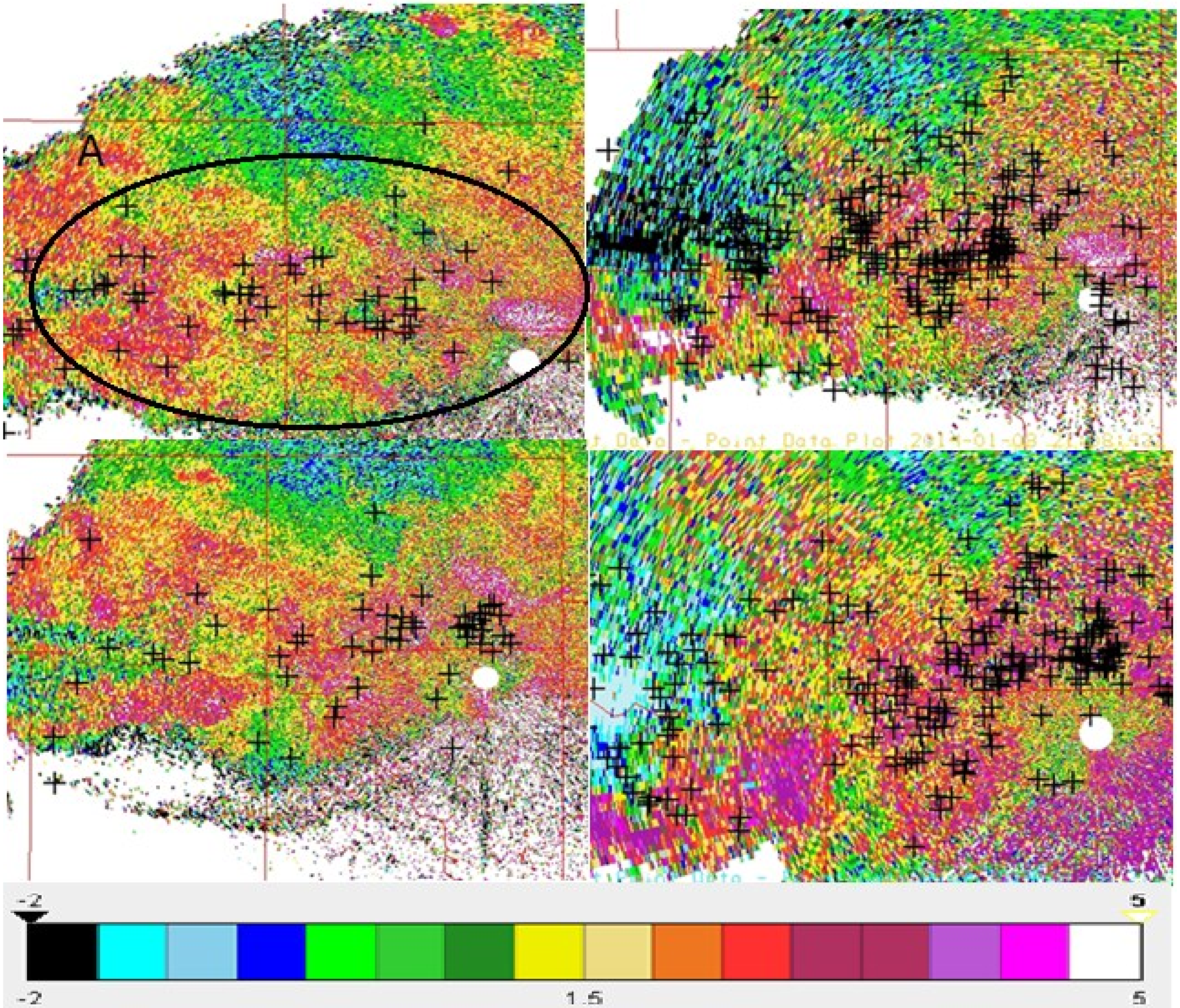

Fig. 11. The left side shows CG strikes during time 3 and the right side shows IC strikes during time 3. The top images are from the first volume scan and the bottom images are from the last volume scan. Region A applies to all images in Fig. 11. The units are dB.

scan in time 3. The first volume scan showed strikes to the northeast of the Z_{DR} ring, with strike locations correlated well to the shape of the ring. The strikes were located in values near 0 to -1 dB. As time progressed throughout this analysis time the strikes appeared on the inside of the ring, while the last volume scan showed strikes inside and outside the ring. This could be from ice particles (inferred from low Z_{DR}) that were charged advecting around and inside the mesocyclone as time progressed. The strikes were not located inside any of the pixels of high Z_{DR}, and were only located in low-Z_{DR} areas.

ρ_{HV}

From Fig. 17, time 1 showed strikes on the outside of low values of ρ_{HV}, which formed a ring. The strikes were located on pixels with ρ_{HV} values around 0.95 with the low values well inside the location of the strikes. The ring of low ρ_{HV} values during time 5 corresponded well to the ring of enhanced Z_{DR} during this time, throughout each volume scan. The first volume scan showed low ρ_{HV} values on the periphery of the enhanced Z_{DR} pixels. This implied that mixed phase particles were present around the high values of Z_{DR} located in the Z_{DR} ring. The strike locations were found immediately on the periphery of low ρ_{HV} values during the last volume scan, with flash locations inside and outside the ring of depressed ρ_{HV}. The high Z_{DR} likely contained supercooled water at this height (elevation angle of 2.4˚) and the low ρ_{HV} indicated mixed phase hydrometeors, which the interactions of the supercooled water and ice particles generating charged particles. As the charged particles followed the cyclonic flow of the mesocyclone on the outskirts of the updraft where sedimentation is encouraged, flashes initiated along the boundaries of the Z_{DR} and ρ_{HV} rings where the separation of charge was enhanced.

V. Conclusions

When differentiating CG strikes from IC strikes, CG strikes

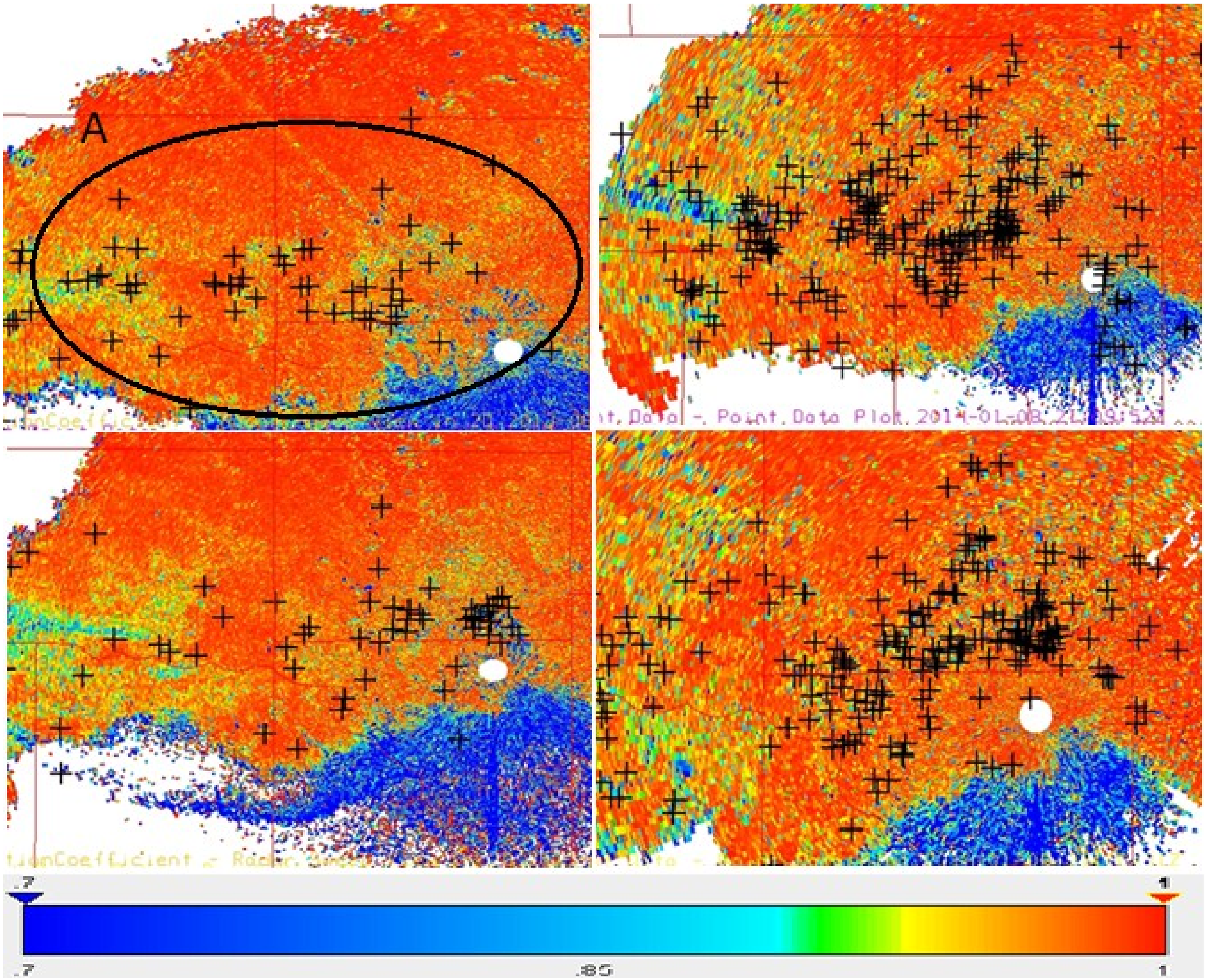

Fig. 12. The left side shows CG strikes during time 3 and the right side shows IC strikes during time 3. The top images are from the first volume scan and the bottom images are from the last volume scan. Region A applies to all images in Fig. 12.

take place in large gradients of reflectivity. This can be related to areas with high sedimentation and wind shear, thus providing charged particles closer to the cloud base encouraging CG flashes. The IC strikes take place either in areas of high reflectivity or on the periphery of these areas, which can be related to hydrometeors being lofted to high elevation, thus discouraging CG flashes and encouraging flashes between charged regions of the storm. Both the number of IC and CG strikes are linked to the areas of the storm with high reflectivity, as these areas are related to intense updrafts where supercooled water can exist along with ice particles and graupel. The areal extent of high reflectivity values on radar PPIs is related to total number of flashes, with larger areas having more flashes and smaller areas having less flashes.

CG and IC flash locations were near areas of high Z_{DR} and K_{DP}, however, they were not located inside these areas but on their periphery. The strikes were located in regions with the strongest gradients of Z_{DR} and K_{DP}, along with mixed values of ρ_{HV}. This implies mixed-phase hydrometeors, which is critical for the non-inductive charging mechanism. The lower Z_{DR} values near higher Z_{DR} correlated well with lower K_{DP} values, which implied ice particles and smaller hydrometeors, which are needed for the riming of graupel in the presence of supercooled water. The lack of strikes collocated with high Z_{DR} and K_{DP} values means charge separation was not encouraged in these regions, as high Z_{DR} and K_{DP} indicated updraft regions were vertical velocities are nearly uniform and little sedimentation of charged particles takes place. This implies the large liquid hydrometeors contain very little if any charge, meaning the charge must be located on the graupel, ice particles, and frozen hydrometeors which the low Z_{DR} and K_{DP} values confirm. The amount of CG and IC strikes are linked to the total areas of high Z_{DR} and K_{DP} values, as the regions with high areas of these polarimetric variables had larger amounts of IC and CG strikes.

In the southern cell which showed large numbers of flashes, high Z_{DR} and K_{DP} values were located above the freezing level throughout each volume scan, with the last volume scan having the largest areas and highest elevations of enhanced

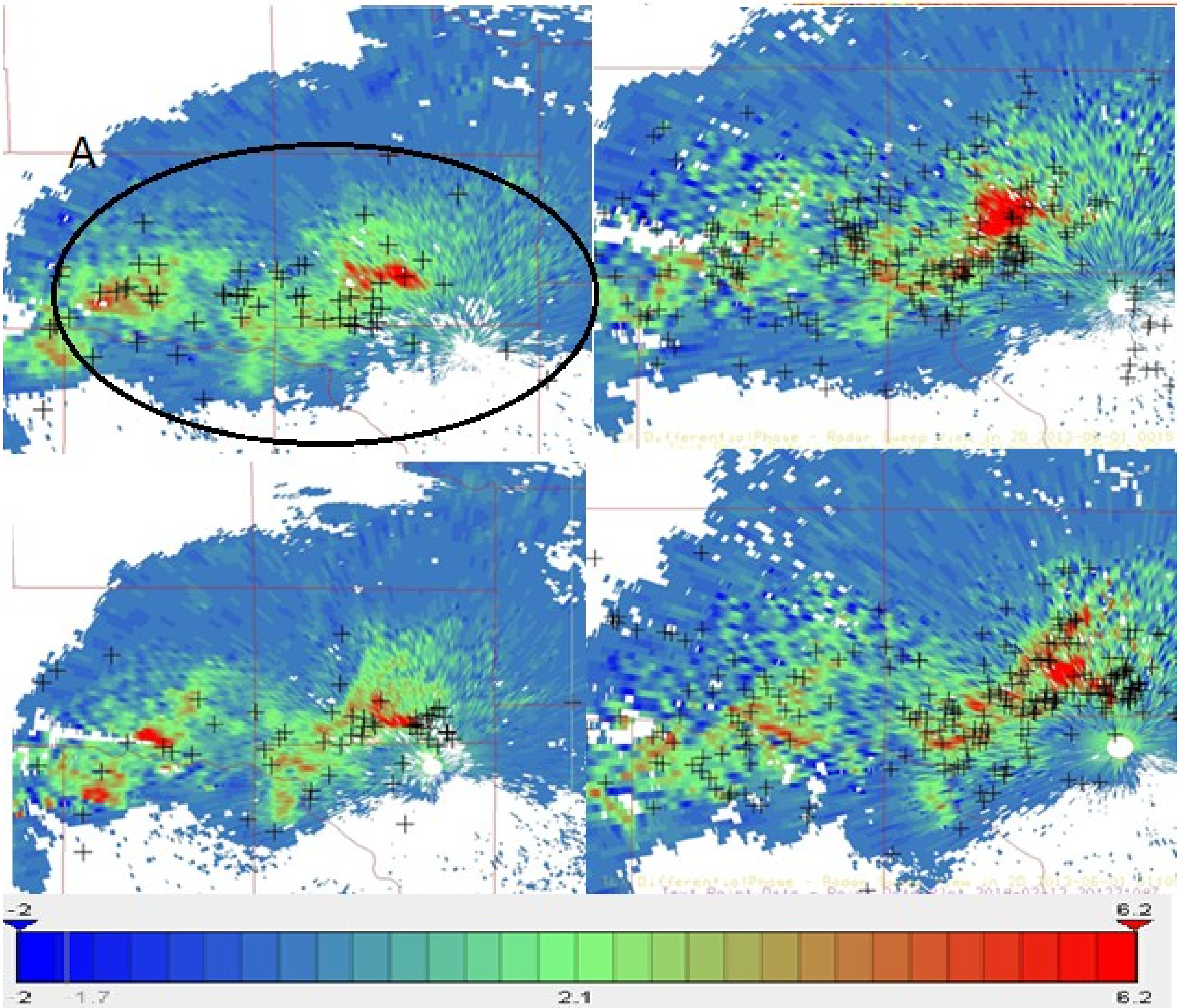

Fig. 13. The left side shows CG strikes during time 3 and the right side shows IC strikes during time 3. The top images are from the first volume scan and the bottom images are from the last volume scan. Region A applies to all images in Fig. 13. The units are deg km^{-1}

Z_{DR} and K_{DP} values. This implies that large amounts of supercooled water were present in this region, which is a necessary condition for the non-inductive charging mechanism.

The southern region showed an increasing amount of high Z_{DR} and K_{DP} values above the freezing level with each volume scan, while the middle region did not show this trend. Both flash rates increased during time 1, however, the southern region had the largest increase in number of flashes with each volume scan during this analysis time. This implies that supercooled water is directly linked to the number of flashes in a region, with larger areas of supercooled water being well correlated with larger amounts of flashes, both IC and CG.

The lightning rings that formed showed strikes on the periphery of Z_{DR} and ρ_{HV} rings. The strikes started on the outside of the Z_{DR} and ρ_{HV} rings and with time moved inside these rings. The strikes avoided the Z_{DR} and ρ_{HV} rings but favored the area immediately outside the rings, implying charged particles on the periphery of these rings which is consistent with Payne et al. (2010). Considering the strikes were located in low Z_{DR} values and high ρ_{HV} values, the particles with charge were likely graupel and ice particles.

Lightning flash initiation points occur along large gradients of Z_{DR}, K_{DP}, and ρ_{HV} in the vicinity of high Z_{DR}, K_{DP}, and Z_{hh} values which corresponds to regions outside updraft areas (which consist of mixed phase particles) above the freezing level. The mixed-phase regions contain a large distribution of hydrometeors, including supercooled water, graupel, and ice crystals which is necessary for the non-inductive charging mechanism. The regions outside of updrafts above the melting level provide supercooled water to ice particles in combination with large vertical velocities gradients, encouraging charge separation and flash initiation. The amount of supercooled water seems critical for the number of flashes in a region, as larger amounts of supercooled water yielded larger flash rates for particular regions.

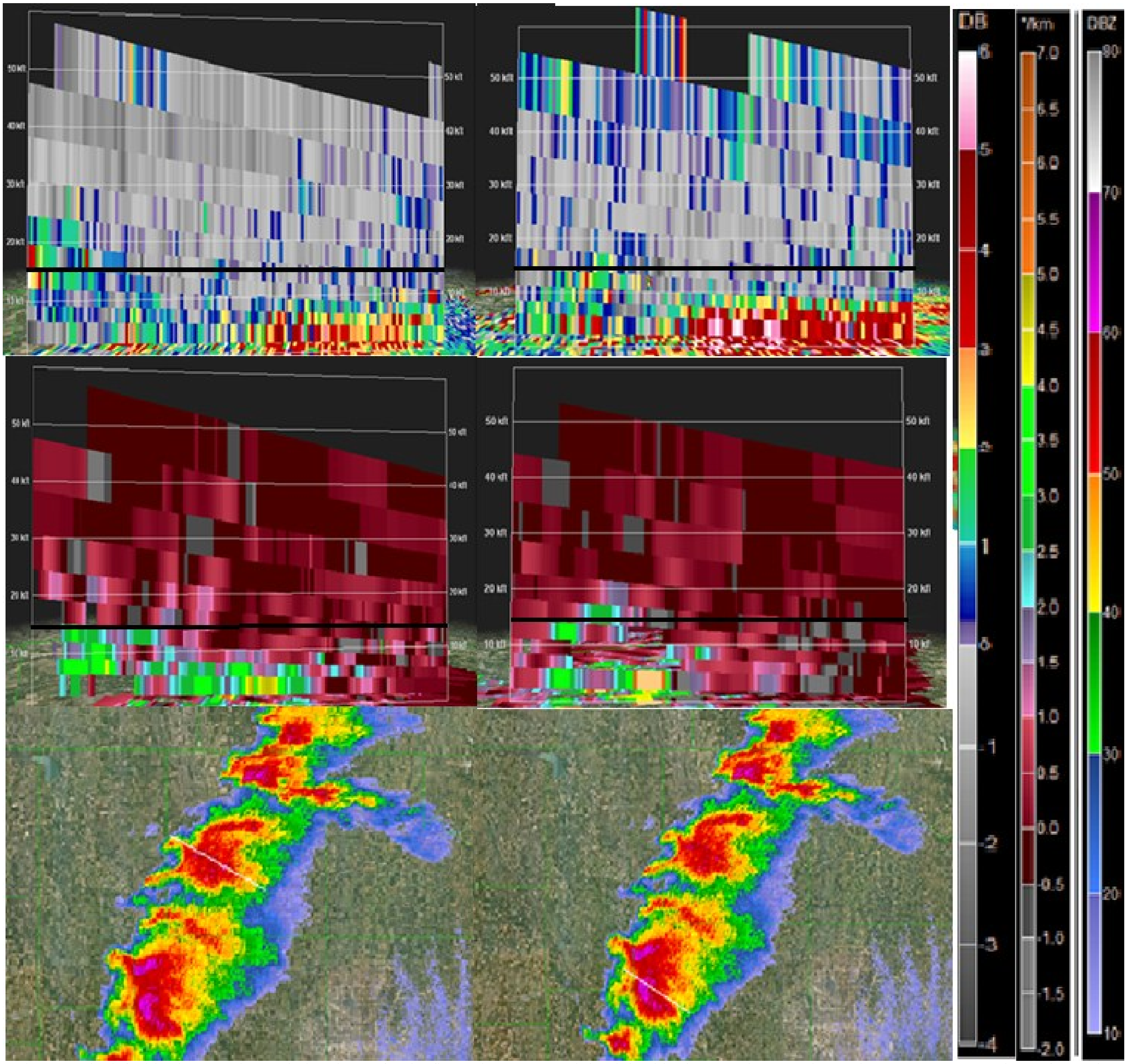

Fig. 14. The left side shows region B during time 1 for the first volume scan and the right side shows region A. The top images are cross sections of Z_{DR}, the middle images are cross sections of K_{DP}, and the bottom images show where the cross sections are located. The black horizontal lines on the cross sections indicate the environmental freezing level, which is approximately 15,000 ft. The legends for the images are to the right; the left most being for Z_{DR}, the middle for K_{DP}, and the right-most for reflectivity. The respective units are listed at the top of each legend.

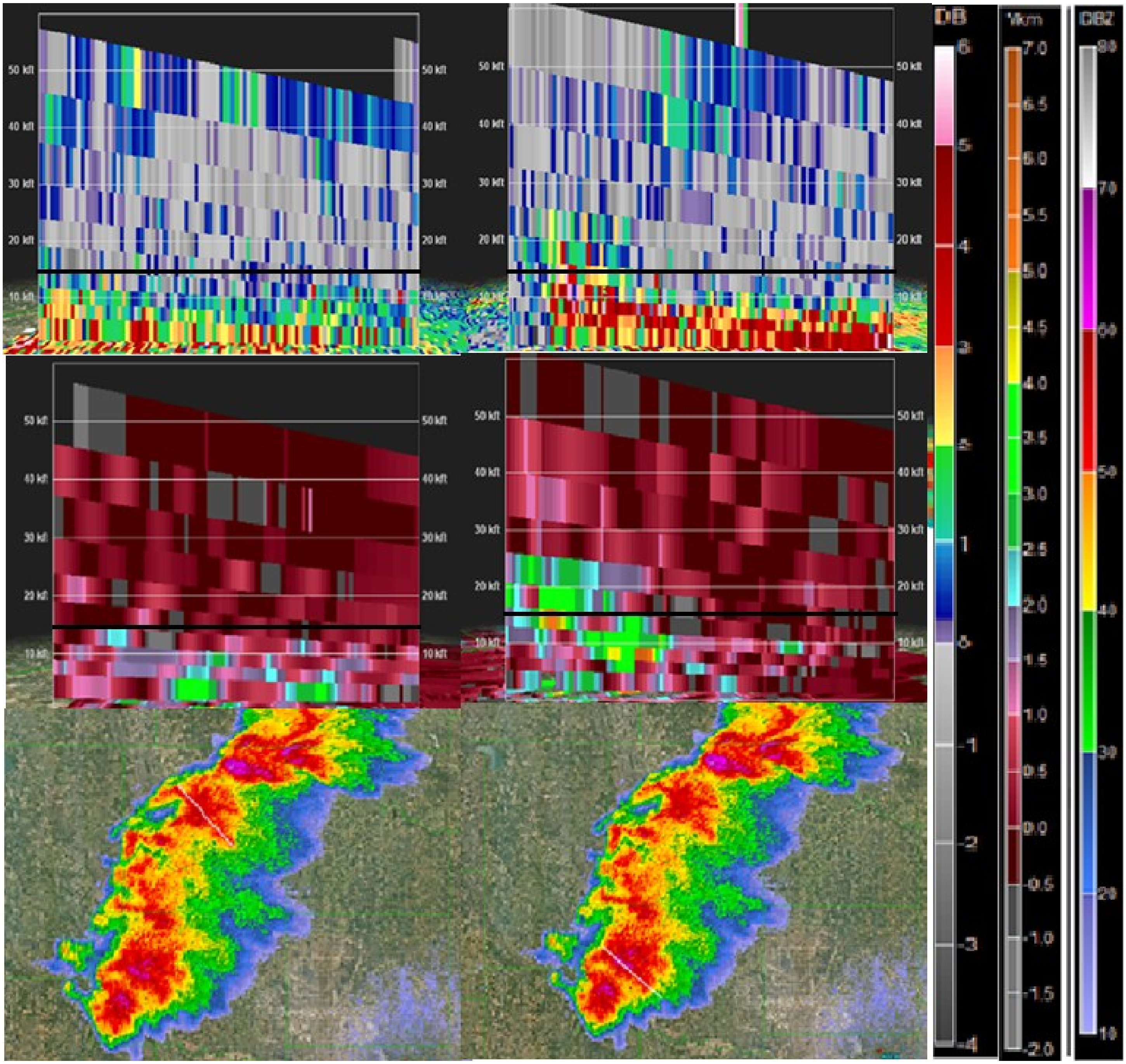

Fig. 15. The left side shows region B during time 1 for the last volume scan and the right side shows region A. The top images are cross sections of Z_{DR}, the middle images are cross sections of K_{DP}, and the bottom images show where the cross sections are located. The black horizontal lines on the cross sections indicate the environmental freezing level, which is approximately 15,000 ft. The legends for the images are to the right; the left most being for Z_{DR}, the middle for K_{DP}, and the right-most for reflectivity. The respective units are listed at the top of each legend.

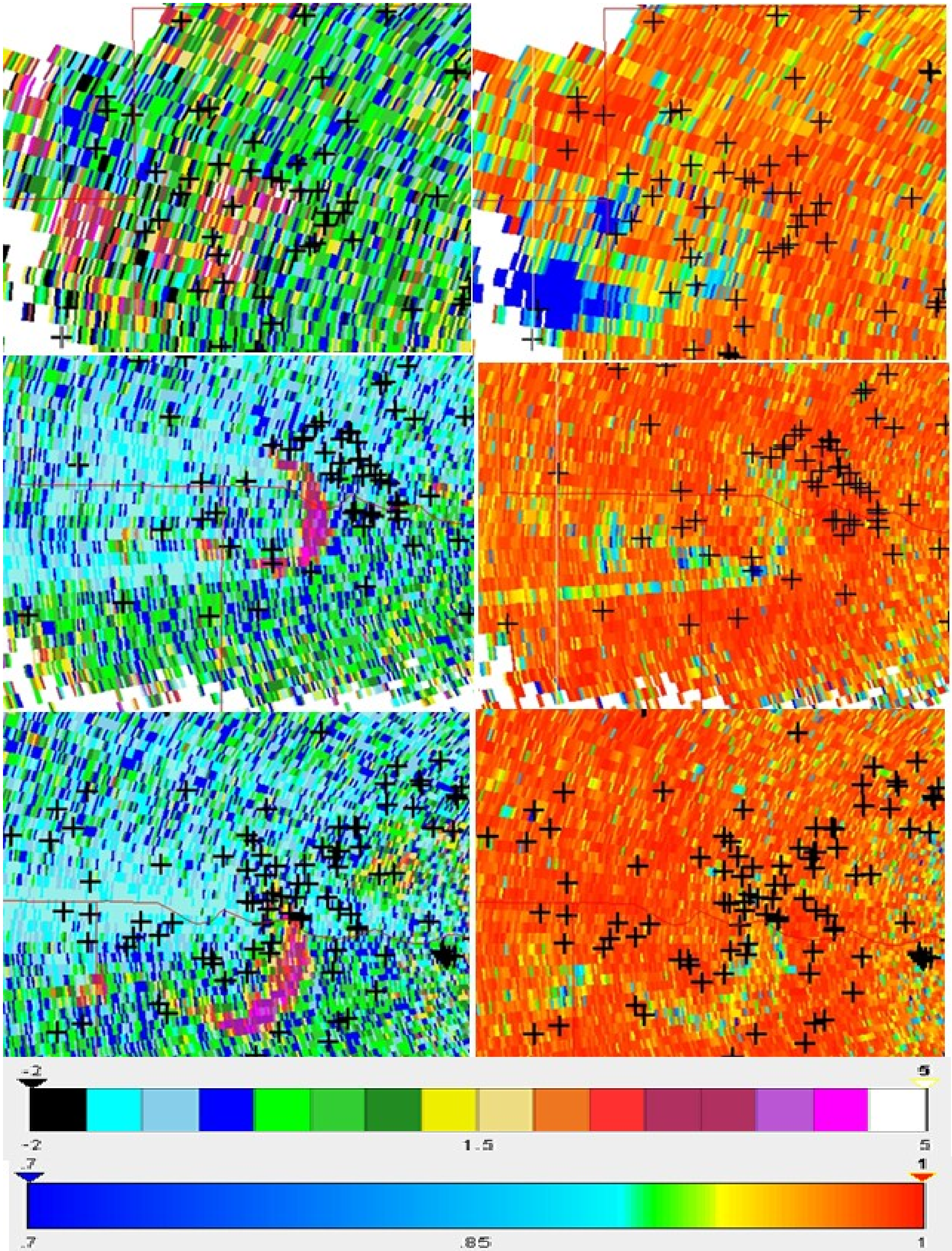

Fig. 16. The top row shows lighting rings for time 1, volume scan 4 with Z_{DR} on the left and ρ_{HV} on the right. The middle row shows lighting rings for time 3, volume scan 1. The left image shows ZDR and the right image shows ρ_{HV}. The last row shows lightning rings for time 3, volume scan 4 with Z_{DR} on the left and ρ_{HV} on the right. The units of Z_{DR} are in dB and ρ_{HV} is unitless.

References

Carey, L.D., S.A. Rutledge (2000), The relationship between precipitation and lightning in tropical convection: A C-Band polarimetric study Mon. Wea. Rev., 128, 2687–2710

Lang, T.J., S.A. Rutledge (2002), Relationships between convective storm kinematics, precipitation, and lightning Mon. Wea. Rev., 130, 2492–2506.

Palucki, J.L., et al. (2011), Comparison between low-flash and non-lightning producing convective areas within a mature mesoscale convective system Wea. Forecasting, 26, 468–486

Payne, C.D., et al. (2010), Polarimetric and electrical characteristics of a lightning ring in a supercell storm Mon. Wea. Rev., 138, 2405–2425

Saunders, C.P.R, (1993), A review of thunderstorm electrification processes J. Appl. Meteor., 32, 642–655

Weiss, S.A., et al. (2008), Evolving complex electrical structures of the STEPS 25 June 2000 Multicell storm Mon. Wea. Rev., 136, 741–756.